Nuclear Science and Techniques (2026) 37:115
https://doi.org/10.1007/s41365-026-01936-z

Study of high-energy neutron-induced fission cross sections using Bayesian methods

Pei-Yan Zhang[1,2] · Zhi-Qiang Chen[1,3] · Rui Han[1,3] · Roy Wada[4] · Guo-Yu Tian[1] · Bing-Yan Liu[1,3] · Hui Sun[1] · Xin Zhang[1] · Rui Guo[1] · Ze-Kun Zhang[1,2] · Qin Li[1,2] · Fu-Dong Shi[1]

Received: 16 June 2025 / Revised: 18 August 2025 / Accepted: 15 September 2025 / Published online: 10 April 2026

Abstract

High-energy neutron-induced fission data for actinide nuclides play a vital role in the foundation for designing advanced nuclear energy systems, such as accelerator-driven subcritical systems and fast neutron reactors. In this study, the INCL++ code was used to calculate neutron-induced fission cross sections in the energy range of 100 MeV–1.2 GeV. Bayesian optimization was employed to refine the parameters in the ABLA++ and GEMINI++ codes, ensuring closer agreement between the computational results and experimental data. We trained a Bayesian neural network using neutron-induced fission data and systematically compared the extrapolations with both theoretical calculations and experimental measurements. The results show that the Bayesian optimization method effectively reduces the chi-squared statistic between the theoretical predictions and the experimental data. Additionally, the Bayesian neural network demonstrates the ability to accurately reflect the trends of fission cross sections when sufficient training data are provided.

Keywords Bayesian neural network · Bayesian optimization · Fission · INCL · Spallation reaction

1 Introduction

The discovery of uranium nuclear fission in 1938 actively promoted the development of human society, such as the utilization of nuclear energy and medical applications. Given the limited uranium resources on Earth, it is of great significance to develop advanced nuclear energy devices such as fast neutron reactors and accelerator-driven subcritical system (ADS). In ADS, a high-energy, intense proton beam generated by an accelerator bombards the target nucleus, inducing spallation reactions and producing external neutrons [1]. These neutrons are then used to drive and sustain the operation of the subcritical reactor, which offers inherent safety advantages over traditional reactors. Accurate and effective nuclear data support is essential for the design of ADS. Neutron-induced fission cross section data can be utilized to investigate the transmutation reaction in ADS, which is a crucial component. Precise neutron-induced fission cross section data of actinide nuclides are crucial for the operation of ADS facilities. Currently, five major evaluated nuclear data libraries (ENDF, JENDL, JEFF, CENDL, and BROND) provide data on the neutron-induced fission of actinides for ADS applications. However, they generally face a shortage of data. The existing data predominantly concentrate on the energy regime below 20 MeV. Within most evaluated nuclear data repositories, a notable deficiency persists in neutron-induced fission cross section data sets for actinide nuclides at energies exceeding 20 MeV [2–5].

Nuclear fission data play a crucial role in basic physics research. They are indispensable for understanding the evolutionary processes of elements in the universe and fusion reactions of superheavy nuclides. Nuclear fission data serve as important inputs for the simulation calculations of the

This work was supported by the National Natural Science Foundation of China (Nos. 12305150 and 11875298).

✉ Zhi-Qiang Chen
zqchen@impcas.ac.cn

1 Institute of Modern Physics, Chinese Academy of Sciences, Lanzhou 730000, China

2 School of Nuclear Science and Technology, University of Chinese Academy of Sciences, Beijing 100049, China

3 Gansu Isotope Laboratory, Lanzhou 730300, China

4 Cyclotron Institute, Texas A&M University, College Station, TX 77843, USA

rapid neutron capture process (R-process) in nuclear astrophysics. Precise calculations of the R-process can enhance the accuracy of the calculated abundances of elements in the universe. Both advanced nuclear energy research and basic physical studies rely on reliable nuclear fission data.

Since its inception in 2001, the neutron time-of-flight (n_TOF) facility at CERN has undertaken a large-scale experimental program, resulting in a wealth of high-quality fission cross section data on actinide elements [6]. In recent years, the China Spallation Neutron Source (CSNS) has also made significant contributions to the measurement of fission reaction cross sections [7, 8]. Owing to the efforts of researchers and advancements in experimental techniques in recent years, the EXFOR database has collected numerous experimental data on the neutron-induced fission cross sections of actinides at energies above 100 MeV. Currently, this includes data for ^{230,232}Th [9–14], ^{233,234,235,236,238}U [10, 11, 15–23], as well as ^{237}Np [10, 17] and ^{239,240,241,242}Pu [10, 24, 25], and ^{243}Am [26]. However, data for other actinide nuclides remain insufficient.

The fission cross sections of actinides were calculated in 2014 by Lo Meo et al. using the INCL++ Liège intranuclear cascade model combined with GEMINI++ and ABLA07 [27]. The (n,f) reaction cross sections of the same nuclide are predicted based on the reaction cross sections of (p,f), and they show generally good agreement with experimental fission cross section data.

With the development of machine learning, these methods have been applied across various fields with promising results. The introduction of machine learning techniques in nuclear data research has gained widespread acceptance. Machine learning can be used to optimize the parameters of physical models, particularly in areas such as nuclear reactions, fission processes, and data evaluation. By training on datasets, machine learning models can predict nuclear parameters and compare them with traditional models, thereby enhancing the assessment of nuclear data. Bayesian neural network (BNN) approaches have been shown to be advantageous for the evaluation of nuclear data when experimental data are insufficient [28–34]. Traditional neural networks often suffer from overfitting when the training data are insufficient, and model predictions tend to exhibit overconfidence. That is, the model outputs appear precise but fail to reflect the results' credibility. In contrast, in BNN, weight parameters are treated as probability distributions rather than fixed values. This allows for the quantification of uncertainty while outputting results, thereby avoiding overconfidence in the model. In regions with missing data, the uncertainty of BNN predictions will reasonably expand, making predictions more robust. The fission reactions induced by high-energy neutrons are divided into two stages. The first is a rapid cascading stage described by INCL++ [35–38]. After the rapid cascading stage terminates, a residual nucleus in an excited state remains, and this residual nucleus de-excites through processes such as evaporation, fission, and radioactive decay. This de-excitation process is described by the C++ versions of the ABLA++ [38–42] and GEMINI++ [43] models.

The rapid cascading stage is represented as a series of two-body nucleon collisions, with Pauli blocking considered during these collisions. Strict blocking is implemented for the first collision, whereas in subsequent collisions, Pauli blocking is applied randomly, with its probability determined by the final-state blocking factor. The INCL model assumes that nucleons in the target nucleus have an independent Woods–Saxon density distribution and that the incident nucleon is located on a spherical surface centered at the target nucleus with a radius of $R_{\max} = R_0 + 8a$, where R_0 and a are the radius and diffuseness of the target nucleus, respectively. This model can self-consistently determine the cascading termination time, which is expressed as $t_{\text{stop}} = 29.8A_{\text{T}}^{0.16}\ \text{fm}/c$, where A_{T} is the mass number of the target nucleus. Owing to this self-consistent definition of the stopping time, the INCL model does not require the inclusion of a pre-equilibrium stage between the rapid cascading and evaporation fission/decay processes.

ABLA++ de-excites residual nuclei through evaporation, fission, and multifragmentation, with the particle evaporation probability using the Weisskopf–Ewing formalism. GEMINI++ tracks a series of binary decays of the residual nucleus until particle evaporation becomes impossible owing to competition from gamma-ray emission. Particle evaporation in GEMINI++ is described by the Hauser–Feshbach evaporation formalism with strict conservation of angular momentum. Compared with the Weisskopf–Ewing formalism used in ABLA++, it has a longer computation time. In ABLA++, the fission width is given by the Bohr-Wheeler transition-state model [44] and follows the Moretto formalism [45]. In GEMINI++, the symmetric fission width is provided by the Bohr–Wheeler transition-state model, whereas the asymmetric fission width is given by the Moretto formalism. The liquid drop barriers in both models were derived from the finite-range model [46]. In the calculation of the level density, ABLA++ employs the constant temperature model of Gilbert-Cameron [47] and the Bethe-type Fermi gas model [48]. GEMINI++ uses a Bethe-type Fermi gas model. Both models can be coupled with INCL++ and contain adjustable parameters.

INCL++ version 6.33.1 was used in this study in conjunction with ABLA++ and GEMINI++ to calculate the neutron-induced fission cross sections of actinides in the range of 100 MeV to 1.2 GeV. Additionally, Bayesian optimization was employed to refine the critical physical parameters and improve the theoretical calculations. We established a BNN model and trained it using the available experimental data and theoretical calculation results.

Subsequently, the output from the trained BNN model was used to compare the theoretical calculation values with the experimental data and to perform analyses.

2 Methods

Bayesian optimization has long been used to address high-cost, black-box optimization problems. It is commonly employed to optimize the hyperparameters of neural network models, effectively reducing computational costs while achieving optimal solutions. A core advantage of Bayesian optimization is that it achieves global optimization with minimal evaluation costs, which significantly enhances the efficiency of parameter optimization. The fission width is expressed as follows:

$$\Gamma_{\mathrm{f}}^{\mathrm{BW}} = \frac{T}{2\pi}\frac{\rho_{\mathrm{sp}}(E-B_{\mathrm{f}},J)}{\rho_{\mathrm{gs}}(E,J)}, \tag{1}$$

where $\rho_{\mathrm{sp}}(E-B_{\mathrm{f}},J)$ and $\rho_{\mathrm{gs}}(E,J)$ denote the level densities of the saddle-point and ground-state configurations, respectively, and T is the nuclear temperature. It can be seen that the fission width is sensitive to $\rho_{\mathrm{sp}}(E-B_{\mathrm{f}},J)$, $\rho_{\mathrm{gs}}(E,J)$, and the fission barrier B_{f}. We will use Bayesian optimization to optimize the parameters in two de-excitation models: ABLA++ and GEMINI++. The parameter to be optimized for the ABLA++ model is $K_{\mathrm{f}}\widetilde{a}$, where K_{f} is a tunable variable and $\widetilde{a}$ represents the asymptotic level density [49] (see formula (2)), and B_{s} is the same as in the liquid drop model. For the GEMINI++ model, the parameter to be optimized is $a_{\mathrm{f}}/a_{\mathrm{n}}$, where a_{f} is the level density parameter at the saddle point and a_{n} is the same quantity at ground-state deformation. The commonly optimized parameter is the fission barrier correction ΔB_{f}. These parameters are regarded as adjustable parameters of the fission model in both GEMINI++ and ABLA++ [27, 43, 50].

$$\widetilde{a} = 0.073A + 0.095B_{\mathrm{s}}A^{\frac{2}{3}} \tag{2}$$

The quality of each set of parameters is evaluated using χ^2, defined as

$$\chi^2 = \sum_{i=1}^{N}\left(\frac{\sigma_{i\mathrm{calc.}}-\sigma_{i\mathrm{exp.}}}{\Delta\sigma_{i\mathrm{exp.}}}\right)^2. \tag{3}$$

In this study, the objective of Bayesian optimization was to minimize the chi-squared error between the experimental points and theoretical calculations, with equal weights assigned to different experimental points. Bayesian optimization is based on Bayes' formula, which is in the following form:

$$P(A|B) = \frac{P(B|A)P(A)}{P(B)}. \tag{4}$$

Among them: $P(A|B)$ is the posterior probability. $P(B|A)$ is the likelihood function. $P(A)$ is the prior probability. $P(B)$ is the marginal likelihood.

A surrogate model of the objective function was constructed using Gaussian processes. The approximate process of Bayesian optimization is as follows: First, several groups of parameters within the set parameter space are determined, and the values of the objective function are calculated. The prior distribution of the surrogate function is initialized according to the calculated values. Based on the prior distribution of the surrogate function and the sampling function, several data points are sampled, and the next evaluation point is selected using the acquisition function. New values of the objective function are obtained according to the sampling results, and the prior distribution of the surrogate function is updated simultaneously. The iteration is repeated to find the global optimal solution. The optimization flowchart is illustrated in Fig. 1.

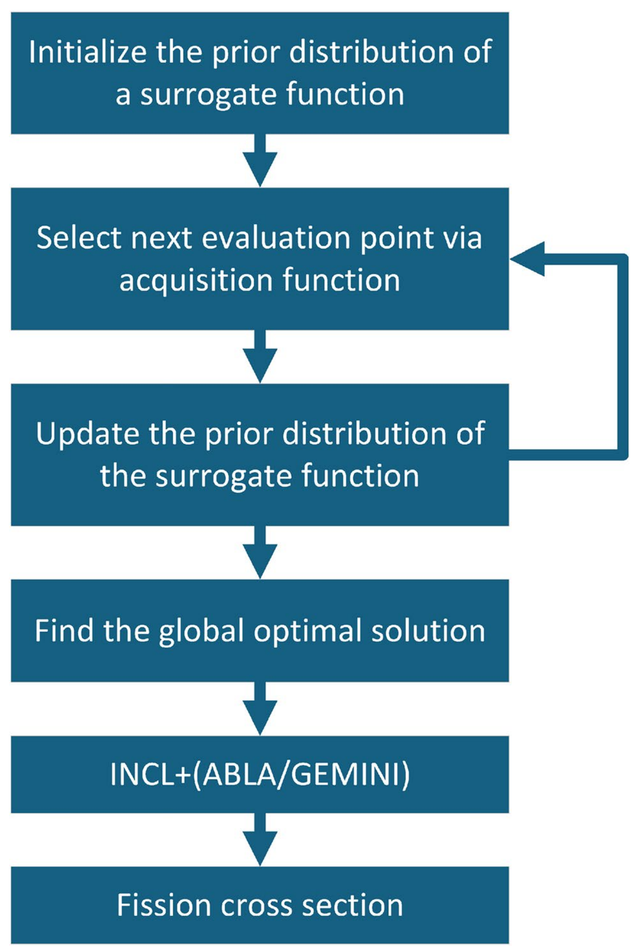

Fig. 1 Bayesian optimization flowchart

There are many third-party Python libraries for implementing Bayesian optimization, such as Bayesian optimization, Scikit-Optimize, and GPyOpt. This study was based on Scikit-Optimize.

The training data for the BNN included experimental data and optimized theoretical calculation results. Among them, the experimental data consist of data above 20 MeV. The data of ^{230}Th measured by B.L. Goldblum et al. above 22.1 MeV were excluded because it has large errors and a seemingly unreasonable trend (see Sect. 3). The theoretical calculation results include the data from ABLA++ and GEMINI++ corresponding to each experimental point at incident neutron energies above 100 MeV, while the theoretical calculation results beyond the range of the experimental data were not included in the training data. The input parameters were the incident neutron energy E, mass number A, proton number Z, and optimized parameters. The parameters in the initial Bayesian neural network follow a normal distribution with an expected value of 0 and a variance of 1. A single hidden layer with a ReLU activation function was used, and the number of neurons was 130. The BNN model was trained using Variational Inference. The Adam (Adaptive Moment Estimation) optimizer was used. Bayesian neural network is based on Pyro implementation. The structure of the Bayesian neural network is shown in Fig. 2.

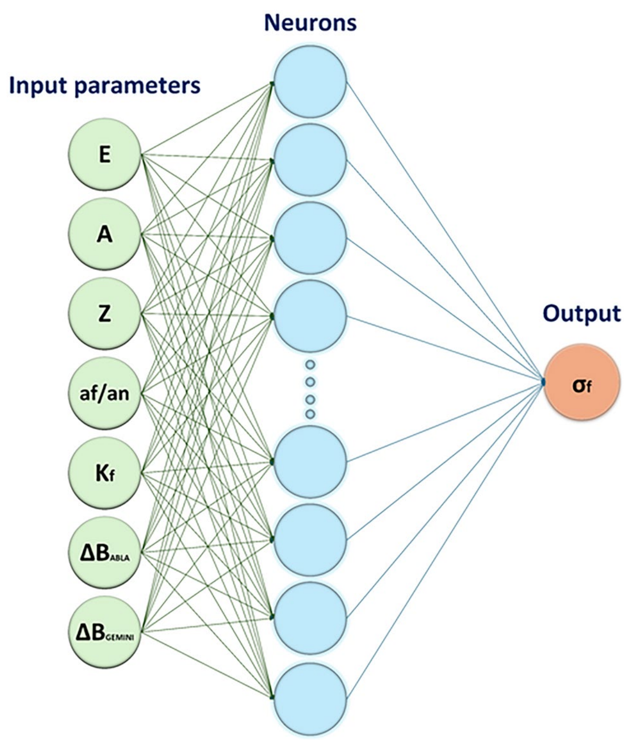

Fig. 2 Bayesian neural network structure

3 Bayesian optimization results

We input the parameters obtained from Bayesian optimization and the default parameters into GEMINI++ and ABLA++ for the calculations. Additionally, we randomly extracted 10 reference experimental points from the Bayesian optimization to compute and compare their χ^2 values. Table 1 presents the parameter results from Bayesian optimization. The direct output of the optimized parameters is given in 16 decimal numbers, but only the first six decimal numbers are effective to the χ^2 value. Comparative calculations indicate that retaining the directly output parameters to

Table 1 Calculation of (n,f) reaction cross sections using GEMINI++ and ABLA++ and evaluation of Bayesian optimization results

Isotope	GEMINI++				ABLA++			
	a_f/a_n	ΔB_f (MeV)	χ^2		K_f	ΔB_f (MeV)	χ^2	
			Optimized	Default			Optimized	Default
^{230}Th	1.073339	0.364485	2.91	202.72	1.7	−0.583926	2.46	563.57
^{232}Th	1.029855	−0.285852	1.19	21.54	0.814365	−0.619712	7.68	158.72
^{233}U	1.061285	0.019202	4.61	65.06	1.018482	−0.367115	6.11	192.92
^{234}U	0.998085	−0.649831	16.21	62.89	0.635090	−0.785347	8.39	61.20
^{235}U	1.026349	−0.378947	1.77	14.73	0.823583	−0.528291	1.43	25.47
^{236}U	1.085907	0.281279	14.01	85.49	1.9	−0.179634	13.79	112.30
^{238}U	1.033683	−0.402918	7.80	100.46	0.903381	−0.460261	7.01	136.22
^{237}Np	0.950680	−1.129486	16.68	143.93	0.578706	−1.077860	6.28	115.25
^{239}Pu	1.012783	0.229608	3.55	55.06	0.8	−0.095793	4.68	10.11
^{240}Pu	1.390086	1.533309	4.58	9.54	0.592403	−0.954778	4.35	101.04
^{241}Pu	0.830721	−0.993972	2.73	22.04	0.316717	−1.503842	1.76	13.71
^{242}Pu	0.889485	−1.027468	17.46	29.86	0.369617	−1.551425	19.57	354.58
^{243}Am	1.118063	1.049270	4.43	22.99	1.700521	−0.156933	3.97	48.11

six decimals has a negligible effect on the χ^2 value. Therefore, we retained the optimized parameters to six decimals and the χ^2 value to two decimal numbers. The default values for parameters in GEMINI++ and ABLA++ are $a_\mathrm{f}/a_\mathrm{n} = 1.036$, $K_\mathrm{f} = 1$, $\Delta B_\mathrm{f} = 0$. Comparing the χ^2 values, it can be seen that using the parameters from Bayesian optimization significantly reduces χ^2. The calculation results are presented in Figs. 3 and 4.

For ^{239}Pu in Fig. 4c and ^{235}U in Fig. 3e, the experimental data for neutron-induced fission cross sections are limited. If only the available neutron-induced fission cross sections are considered, ^{239}Pu and ^{235}U χ^2 can be further reduced. Because the χ^2 values for them include the proton-induced fission cross sections, the following treatment was conducted. Owing to the scarcity of neutron-induced experimental data and the concentration of data below 300 MeV, which cannot fully reflect the overall trend of

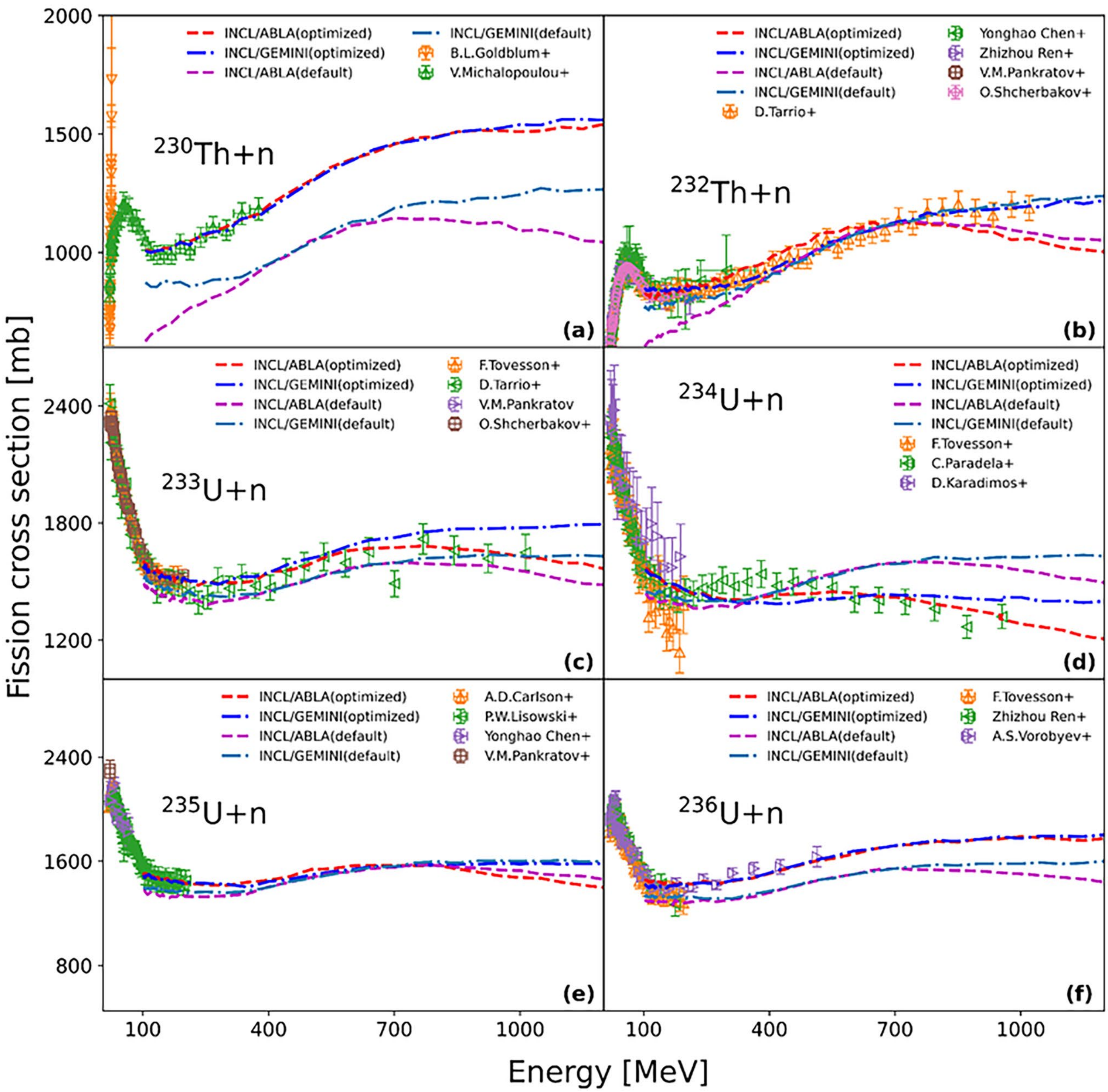

Fig. 3 (Color online) The variations of the total neutron-induced fission cross sections of ^{230,232}Th and ^{233,234,235,236}U with the incident neutron energy

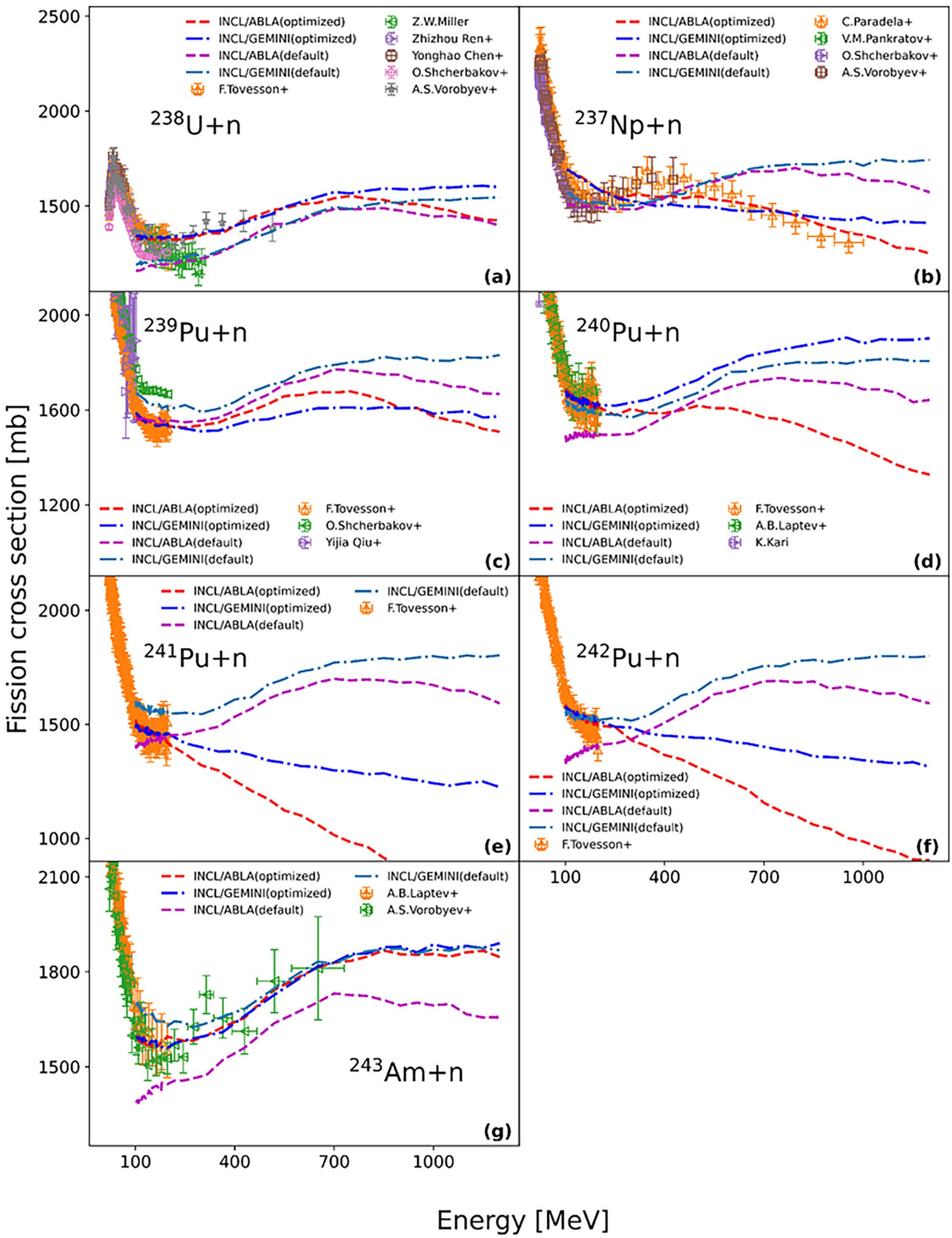

Fig. 4 (Color online) The variations of the total neutron-induced fission cross sections of ^{238}U, ^{237}Np, ^{239,240,241,242}Pu and ^{243}Am with the incident neutron energy

data in the 100 MeV–1.2 GeV energy range, a common issue arises in these nuclei. A similar issue also arises for ^{240,241,242}Pu in Fig. 4d–f, respectively, i.e., theoretical calculations agree well with experiments in energy regions with available data but may appear unreasonable in regions without experimental data.

In Refs. [38, 51], the authors analyzed the correlation between (p,f) and (n,f) cross sections. For the heaviest actinides, the ratio of these two reaction cross sections, that is, $\sigma_{(p,f)}/\sigma_{(n,f)}$, is approximately 1. This could be because the nuclides in this region exhibit similar fission barrier heights, which reduces the sensitivity of the reaction cross sections to the incident channel. The study reported in reference [27] demonstrated that the same parameters could be applied to both (p,f) and (n,f) reactions. Therefore, we added proton-induced fission cross section data for ^{239}Pu and ^{235}U. For ^{240,241,242}Pu, proton-induced fission cross section data are unavailable, precluding their inclusion in Bayesian optimization. Future experimental measurements are anticipated to overcome this limitation.

With the default parameters, the calculated fission cross sections show poor agreement with the experiments in the energy range of 100 MeV–300 MeV, which is most obvious for ^{230,232}Th in Fig. 3a, b and ^{243}Am in Fig. 4g. For ^{234}U in Fig. 3d and ^{237}Np in Fig. 4b, the calculation results with the default parameters significantly overestimate the fission cross sections in the energy range of 500–1000 MeV. The use of the optimized parameters can fix this problem and achieve better agreement with the experimental data. As can be seen in Figs. 3a, b and 4b, there are significant discrepancies between the calculation results of ABLA++ and GEMINI++ above 700 MeV. This may be attributed to the fact that there exists competition between multifragmentation and fission in ABLA++, whereas this is absent in GEMINI++, and that GEMINI++ takes into account asymmetric fission. The optimized parameters were used to calculate the proton-induced fission cross section (see Fig. 5), it is found that, compared with the default parameters [49, 52–61], the optimized parameters increase the fission cross sections at 100 MeV for ^{232}Th as shown in Fig. 5a, ^{233,235,238}U in Fig. 5b–d, and ^{237}Np in Fig. 5e. This may be attributed to the reduction in the fission barrier of the target. For ^{237}Np, the calculation results above 400 MeV with the optimized parameters are lower and exhibit a rapid downward trend because the Bayesian optimization also incorporates the experimental data of neutron-induced fission. In the neutron-induced fission, ^{237}Np shows a steep decline above 400 MeV, which affects the calculation results of the proton-induced fission cross section. It may be insufficient to consider only two parameters for the optimization of ^{237}Np, and other corrections may need to be considered; however, this is beyond the scope of this study.

4 Bayesian neural network results

The dataset was divided into 90% training data and 10% testing data. For the trained BNN model, the mean absolute error (MAE) on the training data was 42.43 mb, and that on the testing data was 40.54 mb. The slight difference between the two MAE values indicates a low risk of overfitting the BNN model. The formula for the MAE is as follows:

$$\mathrm{MAE} = \frac{1}{n}\sum_{i=1}^{n} |y_i - \hat{y}_i|, \tag{5}$$

where y_i is the true value of the i-th sample, $\hat{y}_i$ is the predicted value of the i-th sample, and n is the number of samples.

As shown in Figs. 6 and 7, the neutron-induced fission cross sections are predicted using the BNN model and are denoted by light blue bands around the black solid lines. The blue region represents the 95% confidence interval, and the black solid line denotes the mean value of the probability distribution. The BNN model was extrapolated to incident neutron energies of up to 1.2 GeV and compared with theoretical calculations. For ^{230,232}Th in Fig. 6a, b, the predictions of the BNN model generally agree well with both the experimental data and theoretical calculations. However, for ^{232}Th in the higher energy region, there are significant discrepancies between the predictions of the BNN model and the calculation results of ABLA++. For the ^{233,234,235,236,238}U in Figs. 6c–f and 7a, ^{237}Np in Fig. 7b, and ^{243}Am in Fig. 7g, the predictions of the BNN model show excellent agreement with both the theoretical calculations and the experimental data in the low energy region, where a large amount of experimental data are available. On the other hand, in the higher incident energy region, due to the scarcity of experimental data, there are noticeable differences between the predictions of the BNN model and the calculation results of ABLA++ and GEMINI++. For ^{239,240,241,242}Pu in Fig. 7c–f, the BNN model shows notably wide confidence intervals because the experimental data are concentrated below 200 MeV, and no data are available above 200 MeV, which causes significant discrepancies, making extrapolation results unreliable. Combined with the issues mentioned in the previous section, the lack of experimental data prevents the BNN model from making accurate predictions of the fission cross section trend. However, for nuclides such as ^{230,232}Th and ^{233,234}U in Fig. 6a–d, the comparison between the BNN model extrapolation results and theoretical calculations indicates that the extrapolated trends agree well with the theoretical predictions. We conclude that the BNN model can capture the trends of fission cross section when sufficient training data are available. The correlation between the input features and output cross sections of the

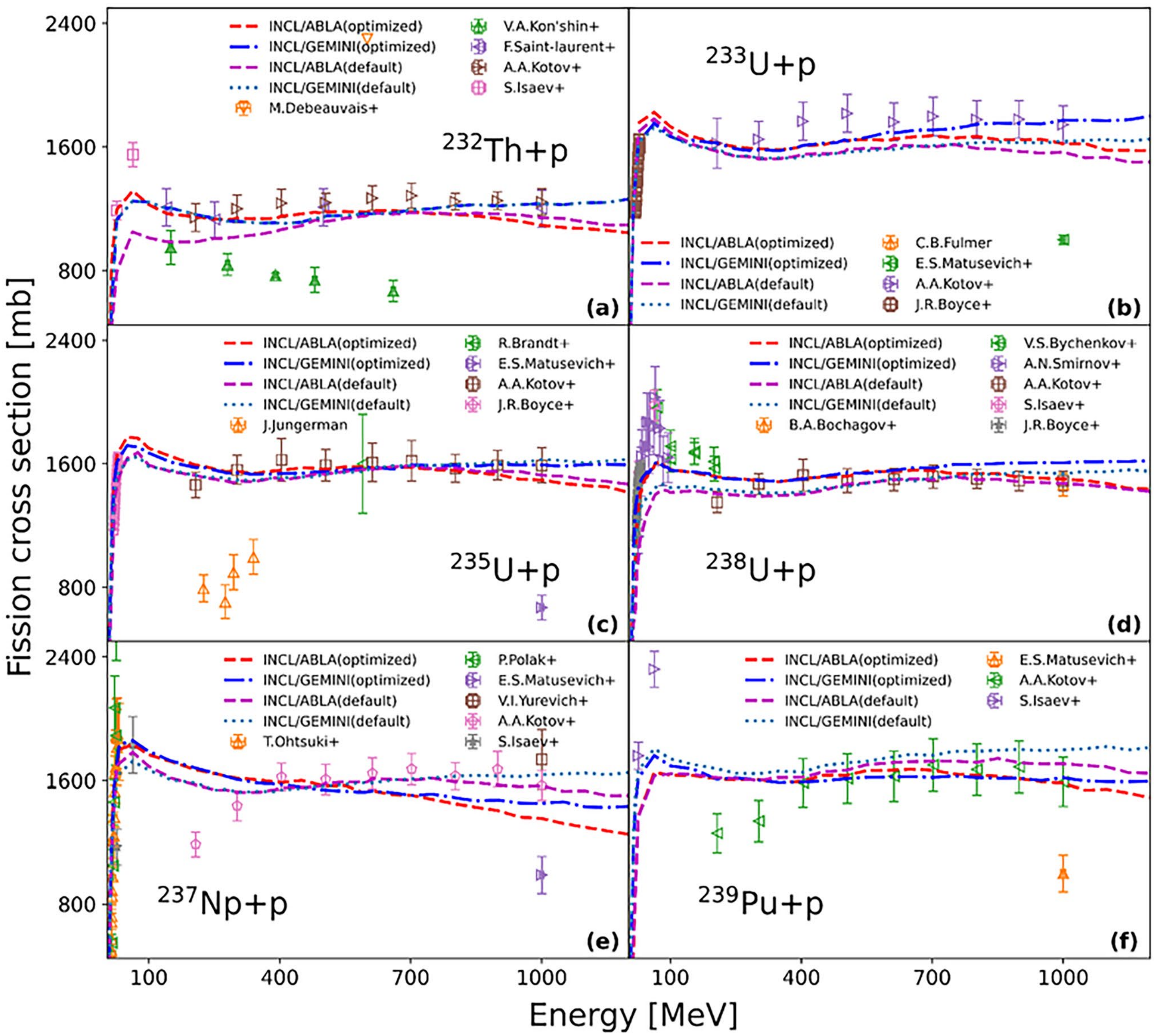

Fig. 5 (Color online) The variations of the total proton—induced fission cross sections of ^{232}Th, ^{233,235,238}U, ^{237}Np and ^{239}Pu with the incident proton energy, and the comparison with experimental data [49, 52–61]

BNN, analyzed using the Pearson correlation coefficient, is shown in Fig. 8. The parameters derived from the Bayesian optimization exhibited a high degree of correlation with each other. Under the condition that the incident neutron energy is less than or equal to 400 MeV, the predicted cross sections of the BNN are highly correlated with the input energy E, target nucleus mass number A, and proton number Z, and negatively correlated with the input energy E. This is similar to the trend that the fission cross sections of most nuclides tend to decrease with an increase in the incident neutron energy below 400 MeV. When the incident neutron energy is greater than 400 MeV, the correlation between the predicted cross sections of the BNN and the incident energy decreases, whereas their correlation with the parameters derived from Bayesian optimization increases.

5 Summary and conclusions

In this study, the INCL++ code version 6.33.1 coupled with the ABLA++ and GEMINI++ models was used within the framework of a BNN model to calculate the total neutron-induced fission cross sections, and the BNN model was established. The Bayesian optimization algorithm was implemented using the Python third-party library

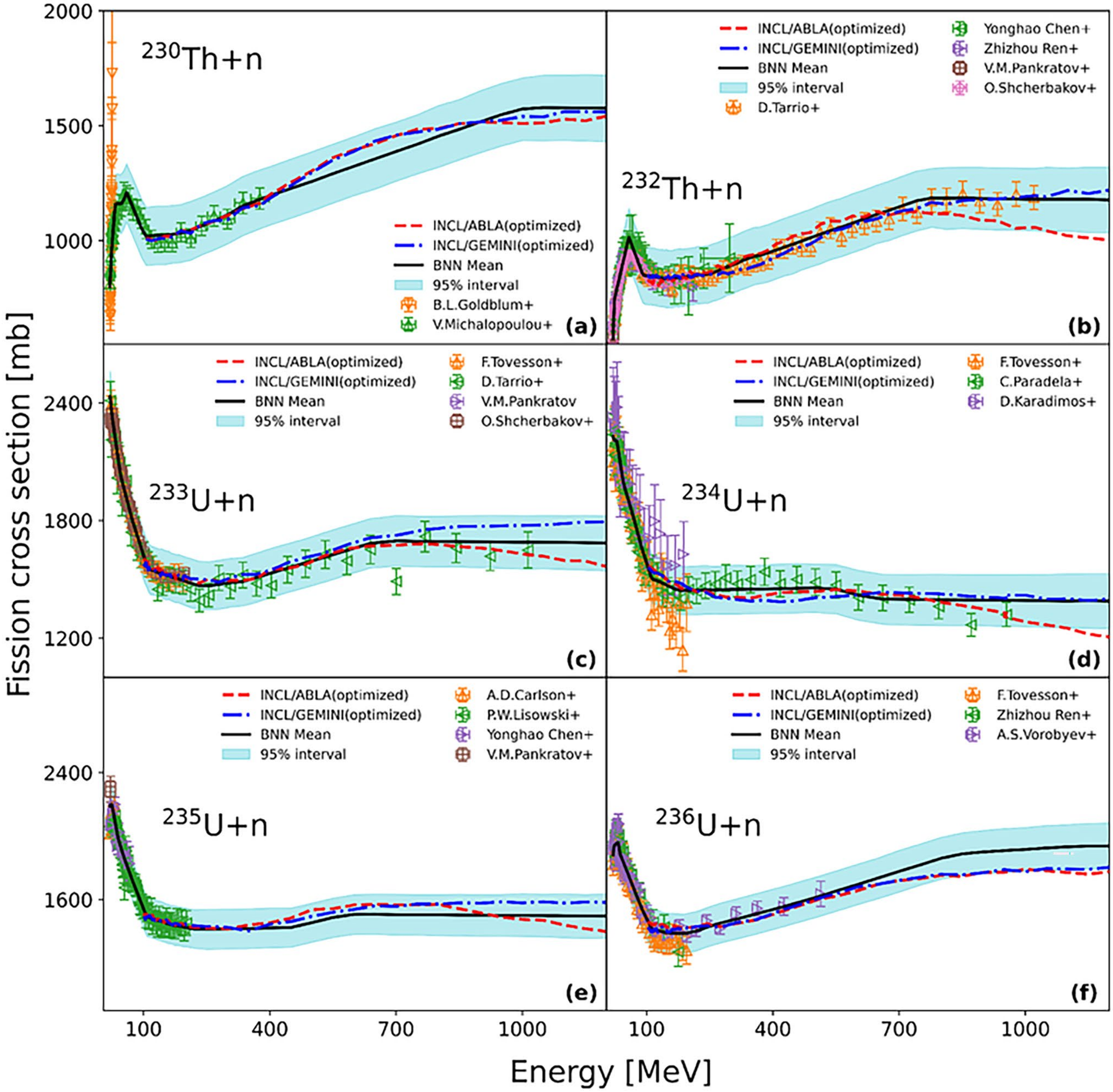

Fig. 6 (Color online) Predictions by Bayesian neural network for ^{230,232}Th and ^{233,234,235,236}U are compared with theoretically computed and experimental data

Scikit-Optimize to optimize the parameters of the ABLA++ and GEMINI++ models. This optimization significantly improved the theoretical prediction of the experimental neutron-induced fission cross sections and demonstrated the potential capability of Bayesian optimization. To avoid the high computational cost and unclear specific form of the objective functions, Bayesian optimization provides an excellent solution. By comparing the extrapolations of the BNN model with theoretical calculations, we concluded that the extrapolations of the BNN model can predict the trends of the fission cross sections when sufficient training data are available. It is hoped that the Bayesian optimization method will be widely applied in future research studies.

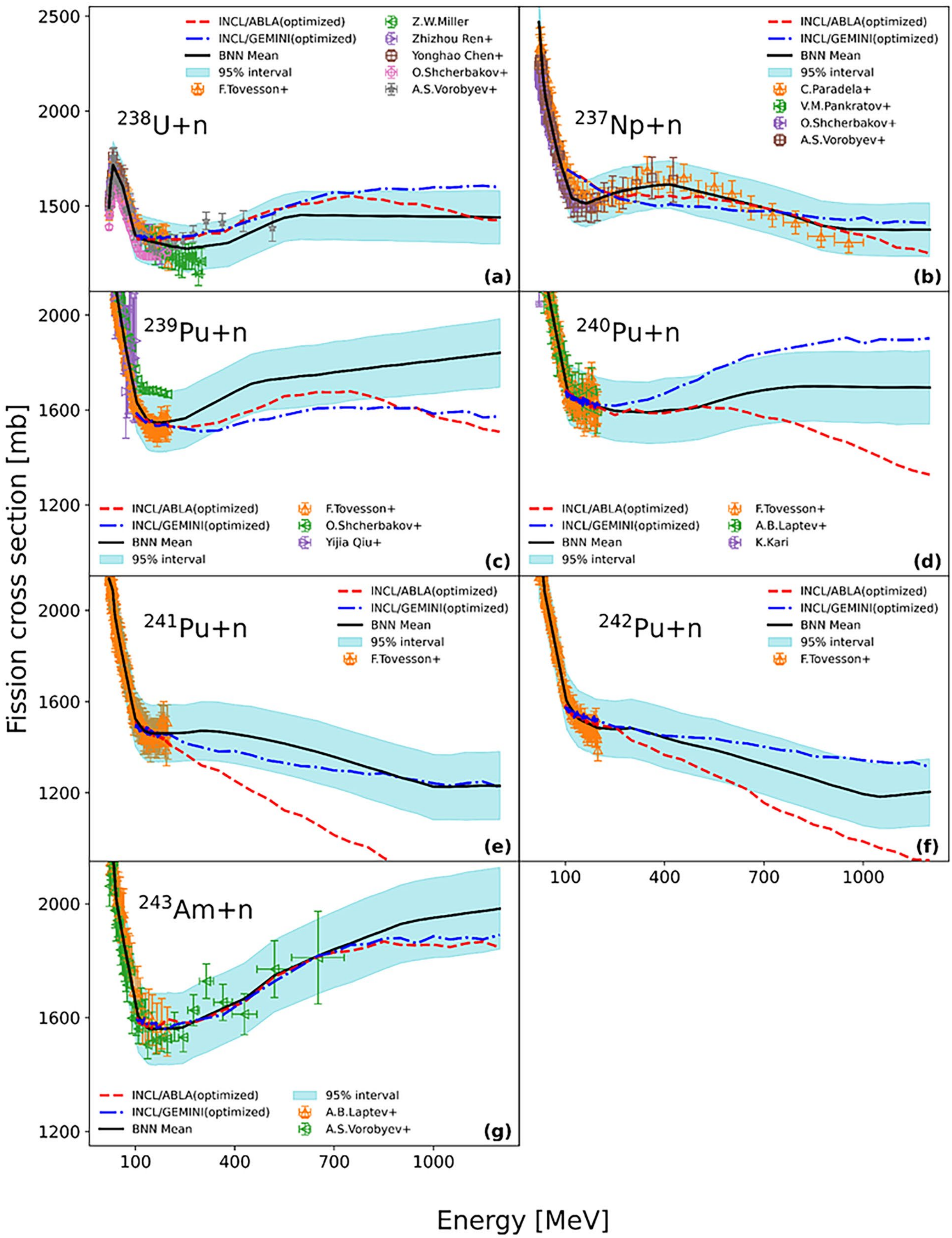

Fig. 7 (Color online) Predictions by Bayesian neural network for ^{238}U, ^{237}Np, ^{239,240,241,242}Pu and ^{243}Am are compared with theoretically computed and experimental data

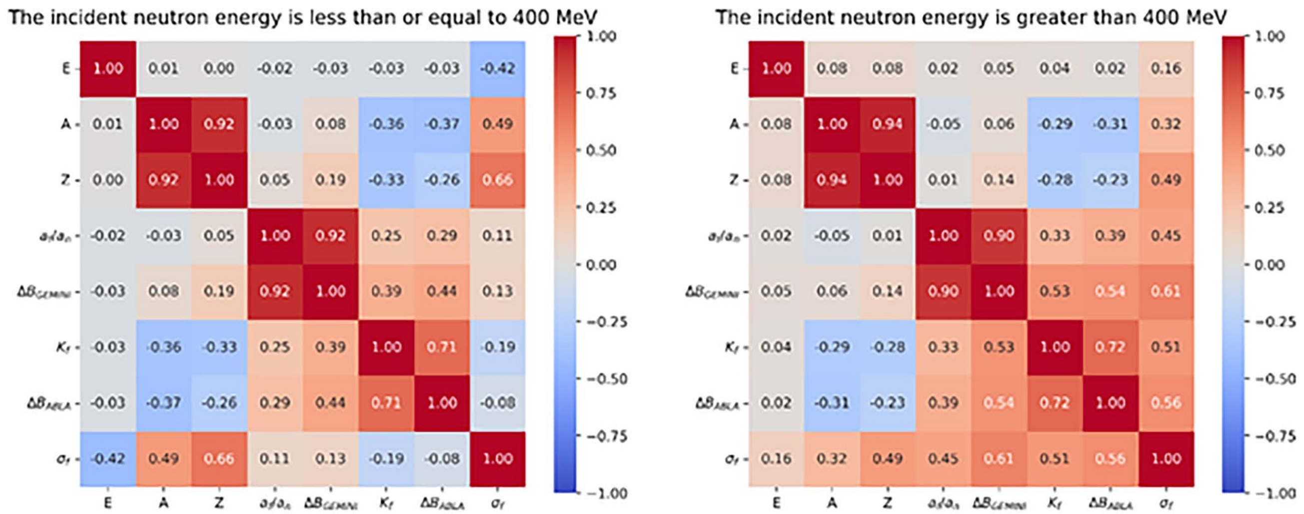

Fig. 8 (Color online) Heatmap of correlation between input features and output cross sections in BNN

Acknowledgements We would like to thank Jean-Christophe David for his support and assistance with this study.

Author Contributions All authors contributed to the study conception and design. Program design, data collection, and analysis were performed by Pei-Yan Zhang. The research methods and ideas were completed by Pei-Yan Zhang and Zhi-Qiang Chen. The first draft of the manuscript was written by Pei-Yan Zhang, and all authors commented on previous versions of the manuscript. All authors read and approved the final manuscript.

Data Availability The data that support the findings of this study are openly available in Science Data Bank at https://cstr.cn/31253.11.sciencedb.j00186.00970 and https://www.doi.org/10.57760/sciencedb.j00186.00970.

Declarations

Conflict of interest The authors declare that they have no conflict of interest.

References

1. W.L. Zhan, H.S. Xu, Advanced fission energy program-ADS transmutation system. Bull. Chin. Acad. Sci. **3**, 375–381 (2012)
2. Z.Q. Chen, Recent progress in nuclear data measurement for ADS at IMP. Nucl. Sci. Tech. **28**, 184 (2017). https://doi.org/10.1007/s41365-017-0335-3
3. S.Y.L.T. Zhang, W.P. Lin, M.R.D. Rodrigues et al., Average neutron detection efficiency for DEMON detectors. Nucl. Instrum. Meth. Phys. Res. Sect. A **709**, 68–71 (2013). https://doi.org/10.1016/j.nima.2013.01.039
4. S.Y.L.T. Zhang, Z.Q. Chen, R. Han et al., Neutron time-of-flight spectrometer based on HIRFL for studies of spallation reactions related to ADS project. Nucl. Sci. Tech. **26**, 030502 (2015). https://doi.org/10.13538/j.1001-8042/nst.26.030502
5. X.Y. Zhang, Y.B. Zhang, F. Ma et al., Neutron production for 250 MeV protons bombarding on thick grain-made tungsten target. Eur. Phys. J. A **51**(8), 106 (2015). https://doi.org/10.1140/epja/i2015-15106-0
6. N. Colonna, A. Tsinganis, R. Vlastou et al., The fission experimental programme at the CERN n_TOF facility: status and perspectives. Eur. Phys. J. A **56**, 48 (2020). https://doi.org/10.1140/epja/s10050-020-00037-8
7. J.Y. Tang, Q. An, J.B. Bai et al., Back-n white neutron source at CSNS and its applications. Nucl. Sci. Tech. **32**, 11 (2021). https://doi.org/10.1007/s41365-021-00846-6
8. J. Wei, H.S. Chen, Y.W. Chen et al., China Spallation Neutron Source: design, R&D, and outlook. Nucl. Instrum. Meth. Phys. Res. Sect. A **600**, 10–13 (2009). https://doi.org/10.1016/j.nima.2008.11.017
9. V. Michalopoulou, A. Stamatopoulos, M. Diakaki et al., Measurement of the neutron-induced fission cross section of ^{230}Th at the CERN n_TOF facility. Phys. Rev. C **108**, 014616 (2023). https://doi.org/10.1103/PhysRevC.108.014616
10. O. Shcherbakov, A. Donets, A. Evdokimov et al., Neutron-induced fission of ^{233}U, ^{238}U, ^{232}Th, ^{239}Pu, ^{237}Np, ^{nat}Pb and ^{209}Bi relative to ^{235}U in the energy range 1–200 MeV. J. Nucl. Sci. Technol. **39**(sup2), 230–233 (2002). https://doi.org/10.1080/00223131.2002.10875081
11. D. Tarrío, L. Tassan-Got, I. Duran et al., Neutron-induced fission cross sections of ^{232}Th and ^{233}U up to 1 GeV using parallel plate avalanche counters at the CERN n_TOF facility. Phys. Rev. C **107**, 044616 (2023). https://doi.org/10.1103/PhysRevC.107.044616
12. Z.Z. Ren, Y.W. Yang, Y.H. Chen et al., Measurement of the ^{232}Th(n, f) cross section in the 1–200 MeV range at the CSNS Back-n. Nucl. Sci. Tech. **34**, 115 (2023). https://doi.org/10.1007/s41365-023-01271-7
13. Y.H. Chen, Y.W. Yang, Z.Z. Ren et al., Measurement of neutron-induced fission cross sections of ^{232}Th from 1 to 300 MeV at CSNS Back-n. Phys. Lett. B **839**, 137832 (2023). https://doi.org/10.1016/j.physletb.2023.137832
14. Y.M. Glenedov, Z. Cui, J. Liu et al., Cross section of the ^{232}Th(n, f) reaction in the MeV neutron energy region. Eur. Phys. J. A **58**, 86 (2022). https://doi.org/10.1140/epja/s10050-022-00716-8
15. F. Tovesson, A. Laptev, T.S. Hill, Fast neutron-induced fission cross sections of ^{233,234,236,238}U up to 200 MeV. Nucl. Sci. Eng. **178**(1), 57–65 (2014). https://doi.org/10.13182/NSE13-56
16. Z. Ren, Y. Yang, R. Liu et al., Measurement of the ^{236,238}U (n, f) cross sections from the threshold to 200 MeV at CSNS

Back-n. Eur. Phys. J. A **59**, 5 (2023). https://doi.org/10.1140/epja/s10050-022-00910-8
17. C. Paradela, L. Tassan-Got, L. Audouin et al., Neutron-induced fission cross section of ^{234}U and ^{237}Np measured at the CERN Neutron Time-of-Flight (n_TOF) facility. Phys. Rev. C **82**, 034601 (2010). https://doi.org/10.1103/PhysRevC.82.034601
18. D. Karadimos, R. Vlastou, K. Ioannidis et al., Neutron-induced fission cross section of ^{234}U measured at the CERN n_TOF facility. Phys. Rev. C **89**, 044606 (2014). https://doi.org/10.1103/PhysRevC.89.044606
19. R. Nolte, M.S. Allie, F.D. Brooks et al., Cross sections for neutron-induced fission of ^{235}U, ^{238}U, ^{209}Bi, and ^{nat}Pb in the energy range from 33 to 200 MeV measured relative to n-p scattering. Nucl. Sci. Eng. **156**(2), 197–210 (2007). https://doi.org/10.13182/NSE06-14
20. A.S. Vorobyev, A.M. Gagarski, O.A. Shcherbakov et al., Measurement of the ^{236}U fission cross section and angular distributions of fragments from fission of ^{235}U and ^{236}U in the neutron-energy range of 0.3–500 MeV. Phys. Rev. C **108**, 014621 (2023). https://doi.org/10.1103/PhysRevC.108.014621
21. V.P. Eismont, A.V. Prokofyev, A.N. Smirnov et al., Relative and absolute neutron-induced fission cross sections of ^{208}Pb, ^{209}Bi, and ^{238}U in the intermediate energy region. Phys. Rev. C **53**, 2911 (1996). https://doi.org/10.1103/PhysRevC.53.2911
22. A.S. Vorobyev, A.M. Gagarski, O.A. Shcherbakov et al., Measurement of the cross section for the neutron-induced fission of ^{238}U nuclei in the energy range of 0.3–500 MeV. JETP Lett. **117**, 557–565 (2023). https://doi.org/10.1134/S0021364023600787
23. R. Nolte, M.S. Allie, F.D. Brooks et al., Cross sections for neutron-induced fission of ^{235}U, ^{238}U, ^{209}Bi, and ^{nat}Pb in the energy range from 33 to 200 MeV measured relative to n-p scattering. Nucl. Sci. Eng. **156**(2), 197–210 (2007). https://doi.org/10.13182/NSE06-14
24. F. Tovesson, T.S. Hill, Cross sections for ^{239}Pu(n, f) and ^{241}Pu(n, f) in the range $E_n = 0.01$ eV to 200 MeV. Nucl.Sci. Eng. **165**(2), 224–231 (2010). https://doi.org/10.13182/NSE09-41
25. F. Tovesson, T.S. Hill, M. Mocko et al., Neutron induced fission of ^{240,242}Pu from 1 eV to 200 MeV. Phys. Rev. C **79**, 014613 (2009). https://doi.org/10.1103/PhysRevC.79.014613
26. A.S. Vorobyev, A.M. Gagarski, O.A. Shcherbakov et al., Measurement of the neutron-induced fission cross section of ^{243}Am relative to ^{235}U in the neutron energy range of 0.3–500 MeV and its analysis. Eur. Phys. J. A **60**, 117 (2024). https://doi.org/10.1140/epja/s10050-024-01334-2
27. S. Lo Meo, D. Mancusi, C. Massimi et al., Fission induced by nucleons at intermediate energies. Nucl. Phys. A **933**, 43–67 (2015). https://doi.org/10.1016/j.nuclphysa.2014.09.040
28. Z.A. Wang, J.C. Pei, Y. Liu et al., Bayesian evaluation of incomplete fission yields. Phys. Rev. Lett. **123**, 122501 (2019). https://doi.org/10.1103/PhysRevLett.123.122501
29. W.F. Li, L.L. Liu, Z.M. Niu et al., Predictions for the (n,2n) reaction cross section based on a Bayesian neural network approach. Phys. Rev. C **109**(4), 044616 (2024). https://doi.org/10.1103/PhysRevC.109.044616
30. Z.S. Jin, M.S. Yan, H. Zhou et al., Bayesian optimization approach to model-based description of α decay. Phys. Rev. C **108**(1), 014326 (2023). https://doi.org/10.1103/PhysRevC.108.014326
31. Z.M. Niu, J.Y. Fang, Y.F. Niu, Comparative study of radial basis function and Bayesian neural network approaches in nuclear mass predictions. Phys. Rev. C **100**(5), 054311 (2019). https://doi.org/10.1103/PhysRevC.100.054311
32. Z.M. Niu, H.Z. Liang, Nuclear mass predictions based on Bayesian neural network approach with pairing and shell effects. Phys. Lett. B **778**, 48–53 (2018). https://doi.org/10.1016/j.physletb.2018.01.002
33. Z.M. Niu, H.Z. Liang, Nuclear mass predictions with machine learning reaching the accuracy required by r-process studies. Phys. Rev. C **106**(2), L021303 (2022). https://doi.org/10.1103/PhysRevC.106.L021303
34. Q.K. Sun, Y. Zhang, Z.R. Hao et al., Enhancing reliability in photonuclear cross-section fitting with Bayesian neural networks. Nucl. Sci. Tech. **36**, 52 (2025). https://doi.org/10.1007/s41365-024-01611-1
35. J. Hirtz, J.C. David, A. Boudard et al., Strangeness production in the new version of the Liège intranuclear cascade model. Phys. Rev. C **101**(1), 014608 (2020). https://doi.org/10.1103/PhysRevC.101.014608
36. A. Boudard, J. Cugnon, J.C. David et al., New potentialities of the Liège intranuclear cascade model for reactions induced by nucleons and light charged particles. Phys. Rev. C **87**(1), 014606 (2013). https://doi.org/10.1103/PhysRevC.87.014606
37. S. Leray, D. Mancusi, P. Kaitaniemi et al., Extension of the Liège Intra Nuclear Cascade model to light ion-induced collisions for medical and space applications. J. Phys. Confer. Ser. **420**, 012065 (2013). https://doi.org/10.1088/1742-6596/420/1/012065
38. J.L. Rodríguez-Sánchez, A. Graña-González, J.C. David et al., Exploring total fission cross sections of neutron- and proton-induced reactions of exotic nuclei at relativistic energies using the INCL-ABLA ++ models. Phys. Rev. C **111**(6), 064606 (2025). https://doi.org/10.1103/PhysRevC.111.064606
39. J.L. Rodríguez-Sánchez, J. Cugnon, J.C. David et al., Hypernuclei formation in spallation reactions by coupling the Liège intranuclear cascade model to the deexcitation code ABLA. Phys. Rev. C **105**(1), 014623 (2022). https://doi.org/10.1103/PhysRevC.105.014623
40. J. Benlliure, A. Grewe, M. de Jong et al., Calculated nuclide production yields in relativistic collisions of fissile nuclei. Nucl. Phys. A **628**, 458–478 (1998). https://doi.org/10.1016/S0375-9474(97)00607-6
41. A.R. Junghans, M. de Jong, H.G. Clerc et al., Projectile-fragment yields as a probe for the collective enhancement in the nuclear level density. Nucl. Phys. A **629**, 635–655 (1998). https://doi.org/10.1016/S0375-9474(98)00658-7
42. J.J. Gaimard, K.H. Schmidt, A reexamination of the abrasion-ablation model for the description of the nuclear fragmentation reaction. Nucl. Phys. A **531**(3), 709–745 (1991). https://doi.org/10.1016/0375-9474(91)90748-U
43. D. Mancusi, R.J. Charity, J. Cugnon, Unified description of fission in fusion and spallation reactions. Phys. Rev. C **82**(4), 044610 (2010). https://doi.org/10.1103/PhysRevC.82.044610
44. N. Bohr, J.A. Wheeler, The mechanism of nuclear fission. Phys. Rev. **56**(5), 426–450 (1939) https://doi.org/10.1103/PhysRev.56.426
45. L.G. Moretto, Statistical emission of large fragments: A general theoretical approach. Nucl. Phys. A **247**(2), 211–230 (1975) https://doi.org/10.1016/0375-9474(75)90632-6
46. A.J. Sierk, Macroscopic model of rotating nuclei. Phys. Rev. C **33**(6), 2039–2053 (1986) https://doi.org/10.1103/PhysRevC.33.2039
47. A. Gilbert, A.G.W. Cameron, A composite nuclear-level density formula with shell corrections. Canadian J. Phys. **43**(8), 1446–1496 (1965). https://doi.org/10.1139/p65-139
48. H.A. Bethe, Nuclear physics B. Nuclear dynamics, theoretical. Rev. Mod. Phys. **9**(2), 69–244 (1937). https://doi.org/10.1103/RevModPhys.9.69
49. V.I. Plyaskin, R.A. Kosilov, Level-density parameters in the back-shifted Fermi gas model. Phys. Atomic Nucl. **63**(5), 752–757 (2000). https://doi.org/10.1134/1.855702
50. S. Lo Meo, D. Mancusi, C. Massimi et al., Monte Carlo calculations of nucleon-induced fission in the GeV energy range. EPJ

Web Conf. **146**, 04049 (2017). https://doi.org/10.1051/epjconf/201714604049
51. A.N. Smirnov, V.P. Eismont, I.V. Ryzhov et al., Proton- and neutron-induced fission cross sections and fission probability in the intermediate energy region. J. Nucl. Sci. Technol. **39**(sup2), 238–241 (2002). https://doi.org/10.1080/00223131.2002.10875083
52. A.A. Kotov, L.A. Vaishnene, V.G. Vovchenko et al., Energy dependence of proton induced fission cross sections for heavy nuclei in the energy range 200–1000 MeV. Phys. Rev. C **74**(3), 034605 (2006) https://doi.org/10.1103/PhysRevC.74.034605
53. S. Isaev, R. Prieels, T. Keutgen et al., Proton-induced fission on actinide nuclei at energies 27 and 63 MeV. Nucl. Phys. A **809**(1), 1–29 (2008). https://doi.org/10.1016/j.nuclphysa.2008.05.012
54. F. Saint-Laurent, M. Conjeaud, R. Dayras et al., Momentum transfer in light-ion-induced fission reactions. Nucl. Phys. A **422**(2), 307–326 (1984). https://doi.org/10.1016/0375-9474(84)90519-0
55. C.B. Fulmer, Total reaction and elastic scattering cross sections for 22.8-MeV protons on uranium isotopes. Phys. Rev. **116**(2), 418–423 (1959). https://doi.org/10.1103/PhysRev.116.418
56. J.R. Boyce, T.D. Hayward, R. Bass et al., Absolute cross sections for proton-induced fission of the uranium isotopes. Phys. Rev. C **10**(1), 231–244 (1974). https://doi.org/10.1103/PhysRevC.10.231
57. J. Jungerman, Fission excitation functions for charged particles. Phys. Rev. **79**(4), 632–640 (1950). https://doi.org/10.1103/PhysRev.79.632
58. R. Brandt, F. Carbonara, E. Cieslak et al., The study of nuclear fission induced by high-energy protons. Rev. Phys. Appl. (Paris) **7**(4), 243–251 (1972). https://doi.org/10.1051/rphysap:0197200704024300
59. P. Polak, A.H.W. Aten, Fission of ^{237}Np by medium energy protons. J. Inorg. Nucl. Chem. **42**(5), 641–653 (1980). https://doi.org/10.1016/0022-1902(80)80209-0
60. V.I. Yurevich, V.A. Nikolaev, R.M. Yakovlev et al., Cross sections for ^{209}Bi, ^{232}Th, ^{235}U, ^{238}U, and ^{237}Np fission induced by intermediate-energy protons and deuterons. Phys. Atom. Nuclei **65**, 1383–1389 (2002). https://doi.org/10.1134/1.1501649
61. T. Ohtsuki, Y. Nagame, K. Tsukada et al., Mass yield curves in low-energy proton-induced fission of ^{233}U, ^{235}U, ^{236}U, ^{237}Np, ^{239}Pu, ^{242}Pu, ^{244}Pu, ^{241}Am, and ^{243}Am. Phys. Rev. C **44**(4), 1405–1423 (1991). https://doi.org/10.1103/PhysRevC.44.1405